CHEMISTRY OF MATERIALS

Article

pubs.acs.org/cm

Versatile Grafting Approaches to Functionalizing Individually Dispersed Graphene Nanosheets Using RAFT Polymerization and Click Chemistry

Yun-Sheng Ye,[†] Yun-Nian Chen,[†] Jing-Shiuan Wang,[†] John Rick,[†] Yao-Jheng Huang,[‡] Feng-Chih Chang,[‡] and Bing-Joe Hwang[†,*]

[†]Chemical Engineering, National Taiwan University of Science and Technology, No.43, Sec. 4, Keelung Rd., Da'an Dist., Taipei 106, Taiwan

[‡]Institute of Applied Chemistry, National Chiao-Tung University, 1001 University Road, Hsin-Chu, Taiwan

Supporting Information

ABSTRACT: Developing powerful and reliable strategies to covalently functionalize graphene for efficient grafting and achieving precise interface control remains challenging due to the strong interlayer cohesive energy and the surface inertia of graphene. Here, we present versatile and efficient grafting strategies to functionalize graphene nanosheets. An alkyne-bearing graphene core was used to prepare polymer-functionalized graphene using 'grafting to' and 'grafting from' strategies in combination with reversible chain transfer and click chemistry. The use of the 'grafting to' approach allows full control over limited length grafted polymer chains, while permitting a high grafting density to a single graphene face, resulting in good solubility and processability. The 'grafting from' approach offers complementary advantages, such as the grafting of high molecular weight polymer chains and a better coverage ratio on the graphene surface; however, the extra steps introduced, the presence of initiating groups, and difficulty in controlling the grafted polymer lead to decreased processability. Various types of polymer chains have been successful covalently tethered to graphene nanosheets using these two approaches, producing various molecular brushes with multifunctional arms resulting in water-soluble, oil-soluble, acidic, basic, polar, apolar, and variously functionalized polymers. This work describes versatile methodologies, using the 'grafting to' and 'grafting from' approaches, for the preparation of individually dispersed graphene nanosheets having the desirable properties described.

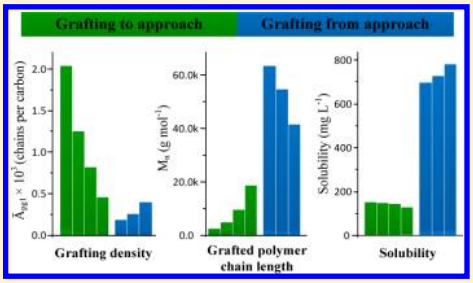

KEYWORDS: *graphene, click chemistry, RAFT polymerization, diazotization*

INTRODUCTION

Due to the unique mechanical, electronic, and thermal properties of graphene, it has been investigated for applications as diverse as high-performance composites,[1,2] molecular electronics,[3] field-emission devices,[4] sensors,[5] and biomedical applications.[6−8] Although graphene can be introduced into some of these applications using *in situ* growth[9] or solid-phase deposition,[10] many others require solution-phase processing and manipulation to achieve the desired assemblies, orientations, and sought after dispersions of the graphene nanosheets within the host material.[11,12] However, the insolubility of graphene in most organic and aqueous solvents adversely impacts the potential for solution-phase processing. Recently, a considerable amount of work has been done to improve the solubility of graphene by covalent coupling[13−15] and the use of noncovalent exohedral electronic interactions[16] to obtain new graphene derivatives for specific applications. Among these approaches, covalent functionalization with polymeric structures is an efficient way to improve the solubility of graphene, and thus, its interfacial interactivity with a target matrix.[17−23] The final properties of graphene can also be adjusted, to satisfy various requirements, by changing the chemical and physical characteristics of the grafted polymer to make it, for example, biocompatible[21,24] or optielectronic,[25] or to introduce gas adsorption properties.[26]

Current approaches for preparing covalent polymer-graphene include the 'grafting to' approach, involving radical coupling[17,23] or reaction with edge-bound carboxylic acid groups on graphene oxide (GO),[25,27] as well as the 'grafting from' approach, which uses initiator-functionalized graphene for polymerization.[20,22,28] The 'grafting to' approach, which involves polymer preparation prior to grafting, allows full control over the molecular weight and polydispersity index (PDI), generally results in low yields with a low grafting density, especially for high molecular weight polymers due to steric hindrance from the attached polymer chains and the relatively low reactivity of the functional groups on the surface of graphene.[29] In order to increase grafting density, relatively harsh grafting conditions, such as high temperatures and long reaction times, are needed, which are detrimental to the

Received: May 2, 2012
Revised: July 23, 2012
Published: July 23, 2012

dx.doi.org/10.1021/cm301345r | *Chem. Mater.* 2012, 24, 2987−2997

functional molecules on either graphene or the polymer. Conversely, the 'grafting from' approach promises a relatively high molecular weight polymer; however, the extra steps needed to introduce the initiating groups on graphene, before polymer grafting for polymerization, make it more difficult to control the polymer's molecular weight, thereby reducing the practicability of the polymerization process.

For the 'grafting to' and 'grafting from' approaches to be successful, several issues need to be addressed. GO is a good starting material for graphene and must be available in large quantities to allow for the scalable functionalization of graphene.[30,31] Although oxygen-containing functional groups (e.g., hydroxyl, carboxyl, and epoxy groups) can assist the dissolution of GO in water and polar solvents, such as tetrahydrofuran (THF), dimethylformamide (DMF), and *n*-methylpyrrolidone (NMP),[32] they may interfere with surface modification reactions. Therefore, a method is needed to introduce specific stable functional groups into graphene. For the coupling of arms, that is, 'grafting to', or for the protection of functionalities used, 'graft from', the reaction must be both relatively mild and highly selective. Finally, using 'grafting from' chemistry (or a method for preparing arms for the 'grafting to' approach), controlled radical polymerization (CRP) is able to yield well-defined polymers with controlled molecular weights, low PDI, and functional group tolerance having high chain-end fidelity. The modification of graphene by diazonium functionalization is emerging as a versatile method for tailoring the chemical and electronic properties of carbon nanotubes[29,33] and graphene.[15,34−36] This chemical handle allows subsequent reactions to attach additional moieties, which will have an important role in introducing reactive functional groups on the graphene sheets' surfaces.[34] The copper-catalyzed Huisgen 1,3-dipolar azide−alkyne cycloaddition reaction has proved to be a versatile method to promote the development of polymer chemistry due to its high specificity, nearly quantitative yield, compatibility with a variety of functional groups, solvent insensitivity, and applicability under mild conditions.[37−39] This reaction has succeeded in grafting various molecules or polymers onto silica materials,[40−42] carbon nanotubes,[29] and graphene.[18,24,34,43,44] We postulated that the combined use of diazonium and click chemistry would be an ideal way to introduce a wide variety of molecules and polymers onto the surface of graphene. For polymerization, reversible addition−fragmentation chain transfer (RAFT) polymerization has attracted significant attention in polymer and materials science due to its versatility and simplicity, where the polymer has a high degree of chain-end fidelity.[45,46] We believe that the combination of click chemistry and RAFT techniques will offer versatile and facile approaches to the covalent functionalization of graphene-based nanocomposites with well-defined polymeric components.

In this paper, we have introduced alkyne groups on the surface of graphene, using diazonium functionalization, as the first step and have then used the resulting alkyne-functionalized graphene (alkyne-FG) as a 'core' material (Scheme S1, Supporting Information). Subsequently, both click chemistry and RAFT polymerization were used to prepare molecular brushes using 'grafting to' and 'grafting from' approaches (Scheme 1). For the 'grafting to' approach, various azido-terminated polymers (polymer-N_3), with a narrow molecular weight distribution, were prepared by RAFT polymerization using azido-terminated chain transfer agents (CTAs-N_3). Subsequently, the polymer chains were grafted onto graphene

Scheme 1. Two Types of Grafting Reactions Used in the Synthesis of Polymer-Functionalized Graphene (Polymer-FG)

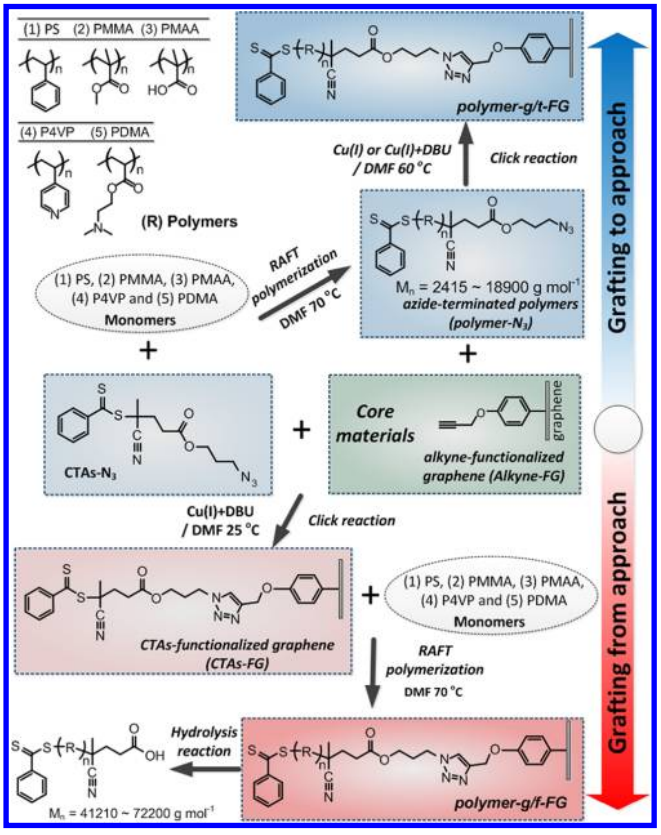

sheets using click chemistry. For the 'grafting from' approach, the CTAs were introduced onto graphene sheets by 'click reacting' CTAs-N_3 with the alkyne groups of the core materials [CTAs-functionalized graphene (CTAs-FG)], followed by RAFT polymerization of linked polymer chains to the graphene nanosheets. This study provides a discussion of each method that includes: (1) the effect of the polymer's chain length and the coupling conditions on the grafting reaction when using click chemistry, (2) how the radical concentration and reaction time controls both the grafted polymer's chain length and grafting density when using RAFT polymerization, (3) the grafting efficiency and characteristics for individual strategies, and (4) the feasibility of extending each strategy to various polymer-functionalized graphenes. We provide valuable information for preparing polymer-functionalized graphenes' using the most suitable conditions for a wide range of potential applications.

■ RESULTS AND DISCUSSION

Synthesis and Characterization of Alkyne-Functionalized Graphene (Alkyne-FG) and CTAs-Functionalized Graphene (CTAs-FG). We prepared the core material (alkyne-functionalized graphene sheets; alkyne-FG) to modify the polymer-N_3 and CTAs-N_3, using a combination of click chemistry and RAFT polymerization.

In this study, the GO nanosheets were produced from natural graphite flakes using a modified Hummer's method, according to a previously reported procedure.[47,48] *p*-Aminophenyl propargyl ether (APPE) was prepared by etherification of *p*-nitrophenol with propargyl bromide, followed by reduction

dx.doi.org/10.1021/cm301345r | *Chem. Mater.* 2012, 24, 2987−2997

to the corresponding aniline derivative.[41] The APPE was subsequently reacted with reduced graphene oxide (R-GO) using a diazotization and coupling procedure[15,22,29,49] under various conditions to produce alkyne-FG. Subsequently, the alkyne-FG and azido-terminated RAFT chain transfer agents (CTAs-N_3) were coupled via [3 + 2] Huisgen cycloaddition, between the alkyne and azide groups, using Cu (I) as catalyst (Scheme S1, Supporting Information).

An overall quantitative picture of the graphene functionalization can be obtained from TGA, see the list in Table S1, Supporting Information. From Figure S1, Supporting Information, it can be observed that GO is not thermally stable; the mass loss of GO started below 100 °C, which can be attributed to the volatilization of stored water in the π-stacked structure.[50] The rate of mass loss increased as the temperature rose to ~200 °C due to the pyrolysis of labile oxygen containing groups, generating CO, CO_2, and steam.[51] On the other hand, R-GO showed an enhanced thermal stability due to the removal of oxygen-containing functional groups by hydrazine reduction. For modified graphene samples, only one weight loss stage at 200−550 °C was observed, resulting from the decomposition of functionalized and unstable groups. In the quantitative analysis, the grafting density of modified graphene ($\bar{A}_{mg}$) can be calculated from eq S1, Supporting Information.[23,52]

The *in situ* functionalization of carbon materials using organic nitrites and aromatic amines has been successfully applied to the functionalization of carbon nanotubes using a solvent-free diazotization procedure.[33,53] However, the grafting ratio of the APPE on graphene nanosheets was not as high as we expected, that is, only 0.61 functinoal groups per 100 carbons using solvent-free conditions. We speculate that the unique confined geometry on graphene's surface may result in less opportunities for surface diazotization in the solvent-free state. In contrast, APPE reacted with a graphene suspension in water using a diazotization had a higher grafting ratio of APPE (>0.95 functional groups per 100 carbons) on the graphene surface. With increasing APPE concentrations, the grafted APPE monomer ratio increases from 0.95 to 1.4 functional groups per 100 carbons and reaches a maximum value of 2.47 functional groups per 100 carbons in the presence of surfactant (SDBS), indicating that the surfactant can prevent agglomeration of the platelets, while simultaneously facilitating surface diazotization. In this study, a core material having the highest grafting ratio of alkyne-FG (2.47 functional groups per 100 carbons) was chosen, as it can substitute a high ratio of CTAs or polymer-N_3 on the graphene. Subsequently, the click reaction was employed to prepare CTAs-FG and showed the number of grafted CTAs to be 1.35 functional groups per 100 carbons, indicating approximately 55% of alkyne groups of alkyne-FG were substituted.

Figure 1 shows the Fourier transform infrared (FTIR) spectra for the alkyne-FG, CTAs-N_3, and CTAs-FG. The absorbance peaks at 1108, 1614, 1740, 2125, and 3282 cm^{-1} can be attributed to C—O stretching, C═C in carboxylic moieties, C═O assigned to skeletal vibrations of unoxidized graphite domains, C≡C stretching, and the C—H stretch of the C—H bond adjacent to the carbon−carbon triple bond, respectively. Additionally, the signals at 1048, 1740, 2098, and 2230 cm^{-1} present in spectrum b, correspond to C═S stretching, C═O in carboxylic moieties, azide bonding, and C—N stretching, respectively. After the click reaction, several new peaks appeared in the spectrum c of CTAs-FG, due to the existence of CTAs in the products. For example, the bands at

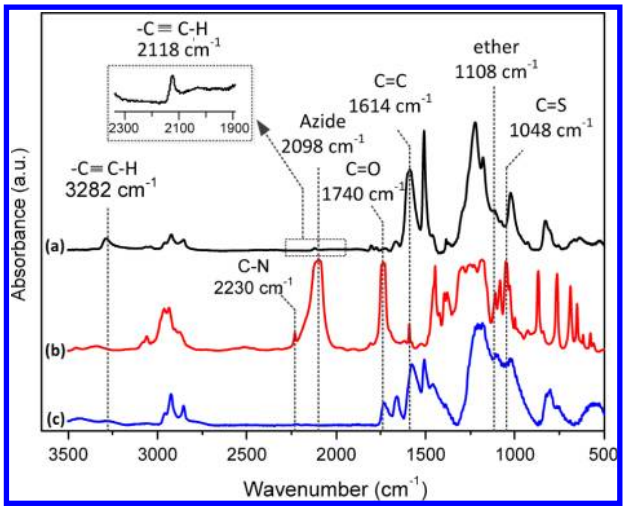

Figure 1. Fourier transform infrared (FTIR) spectra of (a) alkyne-FG, (b) CTAs-N_3, and (c) CTAs-FG.

1048 and 1740 cm^{-1} represent C═S and carbonyl stretching, respectively. The disappearance of the alkyne stretch, after the click coupling, indicates that most of the alkynes have been consumed during this reaction; however, this result is not consistent with the thermogravimetric analysis (TGA) result, as the low intensity of this FTIR absorption may introduce a quantization of conversion error.

C 1s core-level X-ray photoelectron spectra (XPS) of alkyne-FG and CTAs-FG are shown in Figure 2, parts a and b, respectively. Before reduction, the C 1s XPS spectrum of GO (Figure S2a, Supporting Information) clearly indicated a

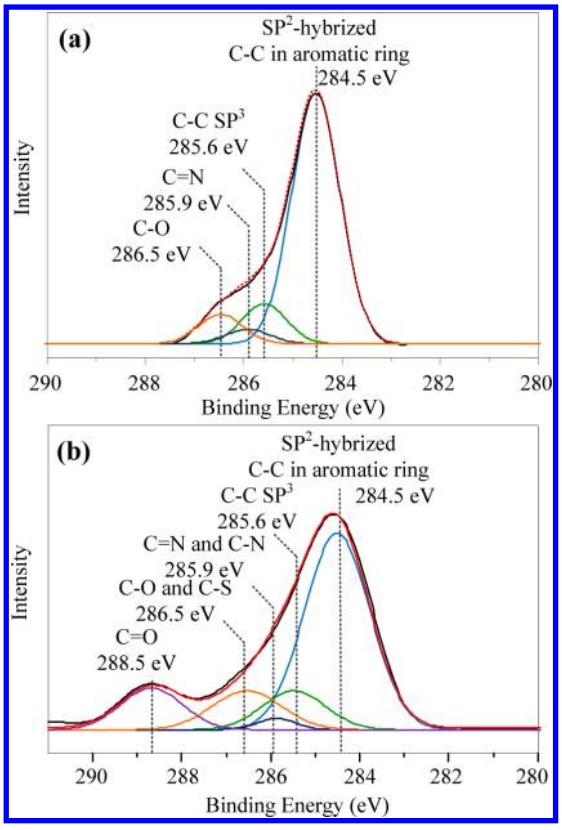

Figure 2. Carbon 1s XPS profile of (a) alkyne-FG and (b) CTAs-FG.

dx.doi.org/10.1021/cm301345r | *Chem. Mater.* 2012, 24, 2987−2997

considerable degree of oxidation with four components, corresponding to carbon atoms in different functional groups, that is, nonoxygenated ring C (284.6 eV), the C in C−O bonds (286.8 eV), the carbonyl C═O (288.5 eV), and the C (epoxy/alkoxy, 286.1 eV).[48] The peak intensities of these components (C—O, C═O, and C—OH) in R-GO (Figure S2b, Supporting Information) are much smaller than those in the GO, indicating considerable deoxygenation during the reduction process. After diazotization, the XPS C 1s core-level spectrum of the resulting alkyne-FG can be resolved by curve-fitting into four peak components with binding energies of about 284.5, 285.6, 285.9, and 286.5 eV, attributable to the sp^2 hybridized C—C in the aromatic ring, sp^3 hybridized carbon, and C═N and C—O species, respectively. The increase in the relative intensities of the sp^3 hybridized carbon and the C—O peak components are consistent with the successful complexing of APPE. After the click reaction, the C 1s core-level spectrum of the CTAs-FG shows a marked increase in the intensity of the sp^3 hybridized carbon, C═N/C—N (285.9 eV) and the C—O/C—S (286.5 eV) peak components, as well as the appearance of the C═O (287.6 eV) peak component. Moreover, a broad signal at 163.5 eV in the S 2p region corresponding to the thio moiety of the CTA appeared, indicating that the CTAs-N_3 have been successfully grafted on the alkyne-FG surface.

Comparison of the alkyne-FG and CTAs-FG ^{13}C NMR spectra provides information about the structures appended on the surface of graphene sheets (shown in Figure 3). The ^{13}C NMR spectrum of GO (Figure S3a, Supporting Information) confirms the presence of abundant epoxide and hydroxyl groups (see, shifts centered at 60 and 69 ppm, respectively), this being in agreement with previous studies.[54] After reduction, the exfoliated GO showed a significant reduction in the amount of epoxide and hydroxyl groups. The peak at 130 ppm shifted to 121 ppm because of the change in the environment of the sp^2 carbons (Figure S3b, Supporting Information). After diazotization, the presence of two distinct resonances dominates the spectrum of alkyne-FG: The resonances centered at 136 and 160 ppm are attributable to the carbons in the phenyl moiety of the propargyl groups, while the small shoulder emerging at 45−90 ppm (not so obvious in the alkyne-FG spectrum) is attributable to the —CH_2—C≡CH group. Finally, the click reaction introduced several new peaks due to the existence of CTAs. For example, ^{13}C NMR revealed peaks at 10−65 and 220−236 ppm respectively representing methyl and methylene carbons of the CTAs and thiocarbonylthio groups [ph—(C═S)—S].

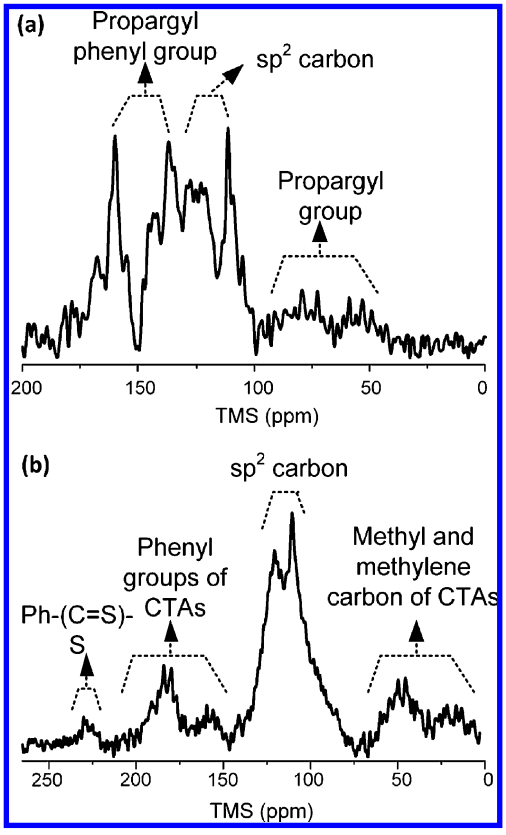

Figure 3. ^{13}C NMR spectra of (a) alkyne-FG and (b) CTAs-FG.

Raman spectroscopic analysis was employed to provide additional structural information with respect to defects in the graphene sheets after oxidation and covalent functionalization. In all samples, two prominent peaks are clearly visible, corresponding to the so-called D (vibration of sp^3) and G bands (vibration of sp^2) at 1330 and 1579 cm^{-1}, respectively.[55,56] In the Raman spectrum of GO, the G band widened and shifted to 1597 cm^{-1} (the G band of pristine graphite is at 1579 cm^{-1}), due to the influence of defects and isolated double bonds.[55] In addition, the D band at 1330 cm^{-1} became prominent, indicating a reduction in size of the in-plane sp^2 domains.[51] The difference in crystallite size L_a of functionalized graphene can provide indirect information about the density of graphene defects.[57] Based on the data in Figure S5, Supporting Information, three crystal sizes were obtained (37.1, 20.8, and 17.7 nm), corresponding to GO, R-GO, and alkyne-FG (Table S12, Supporting Information). After the reduction of GO with hydrazine, the crystallite size of graphene was significantly reduced and was further reduced by diazotization with APPE. This change in crystal size can be attributed to the formation of covalent bonds between graphene and APPE.

'Grafting to' Approach to Graphene Based Molecular Brushes. In our previous study,[40] CTAs-N_3 were synthesized and used to prepare a series of well-defined azido-terminated poly(methyl methacrylates) (PMMA-N_3) by RAFT polymerization. In this study, polymerization of MMA was also mediated by CTAs-N_3, using a small amount of AIBN as the radical source ([AIBN]/[CTAs] <0.2) to avoid deleterious effects on molecular weight control (see the Supporting Information). Table S2, Supporting Information, shows that the correlation between the theoretical and experimental values was excellent, while the narrow and unimodal molecular weight distribution [polydispersity index (PDI) <1.29)] indicates the polymerizations proceeded with good control. The same CTAs were also used, in controlled conditions, for the polymerization of other common classes of vinyl monomers, such as styrene (St), methacrylic acid (MAA), 4-vinyl pyridine (4VP), and 2-(dimethylamino)ethyl methacrylate (DMA) to yield the desired polymer-N_3 (Scheme S2, Supporting Information). The specific conditions utilized for each monomer system and the corresponding results are detailed in Table S3, Supporting Information. The results resemble those obtained for the polymer-N_3 yielding narrow and unimodal molecular weight distributions (PDI < 1.29) and molecular weights (M_n) within the range 8600 to 11200 g mol^{-1} indicating the RAFT polymerization with CTAs-N_3 was well controlled. Repeated washing allowed the facile removal of ungrafted polymer, thereby allowing graphene with covalently grafted polymeric

arms to be quantified by TGA (Figure S4, Supporting Information), while the grafting density of polymer-FG molecular brushes ($\bar{A}_{pg1}$) can be also easily obtained from eq S2, Supporting Information.

By capitalizing on the versatility of RAFT using CTAs-N_3, we are now able to employ click chemistry to prepare a graphene based molecular brush from a wider range of monomers. To successfully implement the click reaction on graphene, the reaction conditions (weight fraction, reaction time, and catalyst type; Table S4, Supporting Information) were optimized prior to conducting the 'grafting to' approach. Comparing entries a, b, and c of Table S4, Supporting Information, provides an indication that higher weigh ratios of PMMA-N_3/alkyne-FG and longer reaction times lead to higher polymer grafting ratios (47.0 wt %). In an attempt to decrease the reaction time and the amount of polymer-N_3 used, while maintaining a high grafting ratio, 1,8-diazabicyclo[5.4.0]undec-7-ene (DBU) was added to the catalyst system. Using this system, it was possible to achieve a higher grafting ratio, that is, comparable to those with only Cu (I), a high weigh ratio of PMMA-N_3/alkyne-FG (20) and longer reaction time (120 h)—this being an effective combination for the click reaction (Huisgen cycloaddition).[53,58] Longer reaction times and higher weight ratios of PMMA-N_3/alkyne-FG under these conditions did not lead to improved grafting ratios. Therefore, we chose a weight ratio of PMMA-N_3/alkyne-FG = 5 reacted for 24 h at 60 °C for the click coupling reaction.

Recently, Gao et al. reported the direct cycloaddition of azide-terminated reagents or azide-terminated polymers to GO using nitrene chemistry and thermolysis of the terminal azide group.[19] Nitrene chemistry was also employed to modify the single walled nanotubes (SWNTs) by cycloaddition of azide-terminated PS.[59] The nitrene chemistry on GO was carried out in NMP at 160 °C under a nitrogen atmosphere, with a reaction time of 18 h. As a control experiment, we attempted to couple our PMMA-N_3 [PMMA-N_3 (100)] to unmodified graphene, R-GO. We found that stirring a mixture of PMMA-N_3, R-GO, and Cu(I) catalysts in DMF at 60 °C for 120 h led to almost no weight change being observed by TGA. Therefore, we can rule out any direct nitrene coupling through the thermolysis of the PMMA-N_3 under our reaction conditions.

The effect of chain length on the grafted polymer's graft density was evaluated by spectrophotometrically estimating the relative solubility of the PMMA-FG in chloroform ($CHCl_3$). In previous studies,[29,53,60] the degree of SWNT solubility, as a result of functionalization, in various solvents was estimated by UV/vis spectroscopy. In this study, we used a similar approach to measure the absorption properties and the degree of solubility of PMMA-FG. A sample of PMMA-g/f-FG (2700) (prepared by the 'grafting from' approach; Table S10, Supporting Information, code 2) was dissolved in 20 mL of $CHCl_3$ and allowed to stand overnight to enable any insoluble material to settle. The supernatant from this solution was diluted several times to produce a total of nine different samples of varying concentration (see the Supporting Information, S8). The absorption spectrum of each of these solutions was then measured, and the absorption value at 500 nm was plotted against graphene concentration (Figure S6, Supporting Information). The slope of the linear least-squares fit of the plotted data provided the specific extinction coefficient, that is, 0.00636, with an R^2 value of 0.995: this data can also be used to estimate the graphene concentration in PMMA-FG/$CHCl_3$.

Comparing the different chain lengths of the PMMA-N_3 grafted to graphene provides an indication that the polymer's molecular weight has an impact on the grafting density of the PMMA-FG molecular brushes (Table S7, Supporting Information). The highest graft density, that is, 2.04 chains per 1000 carbons, was found with a polymer molecular weight of 2415 g mol^{-1} (corresponding to approximately 24 MMA repeat units). This grafting density is higher than that previously reported for 'grafting to' on graphene (1.02 chains per 1000 carbons), assuming a similar polymer chain length (~25 St repeat units).[19] This result indicated that the click coupling reaction is an effective approach to grafting the polymer chain on the graphene surface. Obviously, as the polymer's molecular weight increases, the grafting density decreased (i.e., from 2.04 to 0.46 chains per 1000 carbons) (Figure 4). This result can be

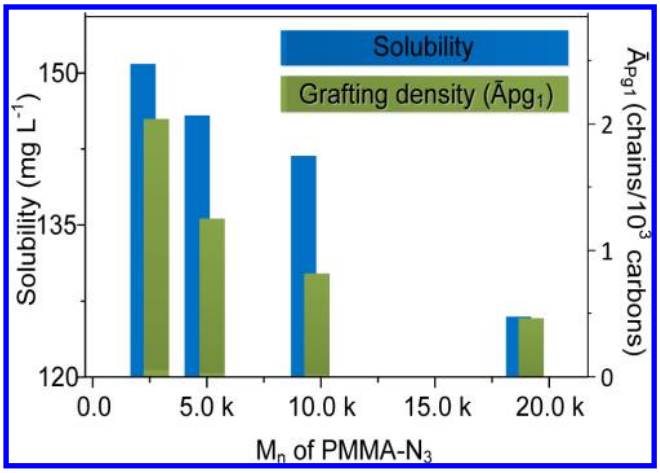

Figure 4. Solubility and grafting density of PMMA-g/t-FG brushes with different PMMA-N_3 average molecular weights (M_n).

explained by the decreased reactivity of the chain-end azide functionality that becomes less accessible as the polymer adopts a more random coil structure at this higher molecular weight.[40]

The incorporation of the polymer chain onto graphene's surface to form graphene based molecular brushes, especially in the 'grafting to' approach, can have two competitive and opposing effects on the solubility of graphene nanosheets. The long polymer chains on the carbon materials trend to improve polymer−solvent interactions and, thus, increase the solubility of carbon based materials. However, with respect to the efficiency of the grafting reaction, long polymer chains generally result in a low grafting density due to the decreased reactivity of the chain-end functionality. In contrast, short polymer chains allow more enhancements to the grafting reaction but are unfavorable to carbon materials dispersed in the solvent due to a reduction in the solubilizing strength of the polymer at lower molecular weights. As illustrated in Figure 4, the solubility of PMMA-g/t-FG (prepared by the 'grafting to' approach) decreases with decreasing grafting densities, even with high molecular weight grafted polymers. Therefore, we believe that the polymer grafting density in PMMA-FG, made by the 'grafting to' approach, dominates the resulting materials' solubility properties.

'Grafting from' Approach Applied to Graphene-Based Molecular Brushes. Controlled/living radical polymerization (CRP) techniques are an effective tool for grafting specific polymer chains onto graphene or GO surfaces.[17,22,61−63] When polymer chains are directly grafted onto graphene or GO sheets

dx.doi.org/10.1021/cm301345r | Chem. Mater. 2012, 24, 2987−2997

by free radical polymerization, it cannot be entirely regarded as a 'grafting from' process, due to the grafting reaction involving a macromolecular radical linked to the double bonds of graphene or GO (i.e., it belongs to the 'grafting to' approach).[23,62] The 'grafting from' approach, usually needs pretreatment to introduce initiating groups on graphene or GO sheets before polymer grafting for CRP. In this study, we employed click chemistry to modify graphene's surface, as described, so that the RAFT agents were covalently linked to the nanosheets' surfaces. Subsequent RAFT polymerization allowed polymer chains to grow from these surfaces. The preparation process illustrated in Scheme S4, Supporting Information, summarizes the experimental results found in Tables S9–S11, Supporting Information.

The most important challenge in the synthetic strategy used here was to maintain control of the grafting density of the arms. GPC was found to be a powerful tool for observing the length of arms attached to the graphene surface. For the M_n determination, the grafting PMMA chains were cleaved from PMMA-FG [PMMA-g/f-FG (2700)] by a hydrolysis reaction involving the ester group between PMMA and graphene. With increasing reaction times, the M_n of grafted PMMA chains increased from 10005 to 63440 g mol^{-1}, while the PDI was slightly reduced from 1.92 to 1.87. However, the PDI of cleaved PMMA is much broader than the PDI value obtained from the RAFT polymerization using CTAs-N_3 (polymer-N_3). Although the exact reason for this phenomenon is not clear, we speculate that a combination of the unique confined geometry of the anchored intermediate macro-RAFT radical on the graphene surface may contribute to uncontrolled chain radical termination.

The data in Figure 5 and Table S9, Supporting Information, show the grafting ratio increasing from 49.3 to 64.4 wt % with

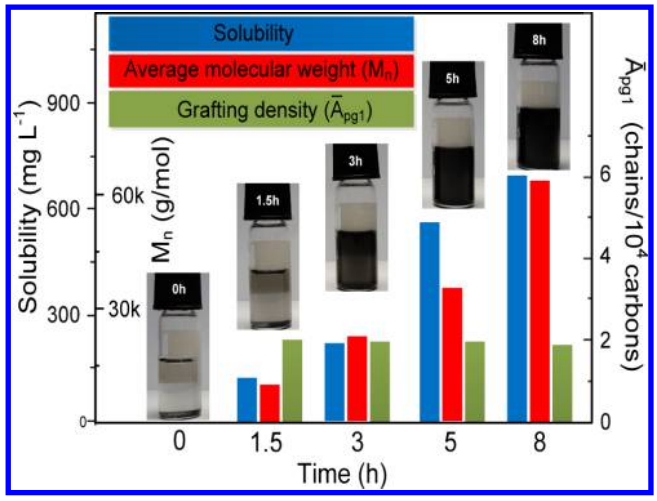

Figure 5. Photographs, solubility, M_n, and grafting density of PMMA-g/f-FG (2700) at different reaction times.

increasing polymerization time. There are two possible reasons that may be responsible for this: (1) an increase in the grafting density and/or (2) the chain length of the grafted polymer on the graphene nanosheets. As mentioned, the polymer chains can be directly grafted onto the graphene, or GO sheets, via free radical polymerization,[23,62] which may also occur in our system due to the use of high concentrations of radical in the RAFT polymerization. As a control experiment, we attempted directly polymerizing PMMA onto unmodified graphene, R-GO. We found that even with higher concentrations of AIBN ($[M_0]/[I]$ = 625) in our control polymerization, the reaction products had a very low solubility (34 mg L^{-1}; Table S10, Supporting Information, code 1) and a slight difference in weight loss at 800 °C when compared to R-GO (Figure S10, Supporting Information). The grafting density of the PMMA-g/f-FG can be also obtained from the previous method. The calculated result showed only a slight variation in grafting density (1.90–2.01 chains per 10000 carbons. Figure 5), shows only traces of macromolecular radical coupling in our RAFT polymerization. From these results, the increase in the chain length of the grafted polymer with polymerization time is the most important contribution to the increased grafting ratio and is also reflected in the solubility of the resulting PMMA-FG. As expected, the increasing chain length of the grafted polymer significantly improved the polymer's 'solubilizing' strength and increased the solubility of PMMA-FG, which reached its maximum solubility of 695 mg L^{-1} after 8 h.

Besides adjusting the time, we also tried to adjust the chain length of PMMA-FG by changing the molar ratio of monomer to initiator ($[M_0]/[I]$) during RAFT polymerization. The chain length of the grafted polymer and the grafting density were determined by GPC and TGA; see the experimental results in Table S10, Supporting Information. The results showed that the chain length of the grafted polymer can be slightly modulated by increasing the initiator concentration; however, the grafting density will change simultaneously. The increase in grafting density with increasing concentrations of initiator may result from increasing opportunities for radicals transfer to the CTAs of graphene and produce a greater degree of polymer chain progration from the surface. When the chain length of the grafted polymer remained a specific length (M_n > 41500 g mol^{-1}), the change of grafting desnity of PMMA on graphene was directly apparent in the weight loss behavior. Figure S10, Supporting Information, shows TGA curves for the PMMA-g/f-FG brushes with different $[M_0]/[I]$ ratios under the same conditions. For the three PMMA-g/f-FG samples, the thermal stability improved with increasing grafting densities; decomposition was thus not apparent until ~250 °C. Increasing thermal stability with increasing grafting density indicates that a higher grafting density of PMMA layers inhibits the decomposition of residual groups on CTAs-FG more effectively, due to the larger coverage ratios of the polymer layers.

Characteristics of Graphene Based Molecular Brushes and Their Composites by 'Grafting to' and 'Grafting from' Approaches. The successful combination of click chemistry and RAFT polymerization was confirmed by FTIR, XPS, and ^{13}C NMR measurements. Figure S7, Supporting Information, shows FTIR spectra for the alkyne-FG, CTAs-FG, and PMMA-FG. After functionalization, the grafting reaction increased the intensity of several peaks including C—O—C stretching (1108 cm^{-1}), C—O stretching (1258 cm^{-1}), and C═O in carboxylic functions (1740 cm^{-1}), due to the introduction of PMMA. The intensity of these absorbance peaks was more obvious in the PMMA-g/f-FG (625), which is attributed to the higher grafting ratio (grafting ratio of PMMA-g/t-FG (200) = 55.5 wt % and PMMA-g/f-FG (625) = 70.9 wt %) and the longer grafted PMMA chains (M_n of PMMA-g/t-FG (200) = 18900 g mol^{-1} and PMMA-g/f-FG (625) = 41500 g mol^{-1}) increasing the relative PMMA intensity in PMMA-FG. The XPS C 1s core-level spectral comparison between PMMA-FG and functionalized graphene (alkyne-FG and CTAs-FG)

dx.doi.org/10.1021/cm301345r | Chem. Mater. 2012, 24, 2987–2997

provides further information about the PMMA structure appended to the surface of graphene sheets (shown in Figure S8, Supporting Information). A new peak component at 288.5 eV indicates the presence of the C═O species formed by grafting PMMA on the graphene's surface. Structural characteristics of the grafted PMMA can also be observed by ^{13}C NMR (Figure S9, Supporting Information) and shows that the PMMA methyl and methylene carbon peaks (12.5−50 ppm) appear in the PMMA-FG. In previous studies,[20−22,64] the I_D/I_G ratio or crystallite size in Raman spectra was used to confirm the formation of covalent links between the graphene sheets and grafted polymer chains. However, in our approach, the crystallite sizes (L_a) of PMMA-FG [17.8 for PMMA-g/t-G (200) and PMMA-g/f-FG (625)] are almost unchanged after grafting relative to the alkyne-FG (L_a = 17.7 nm) (Table S12, Supporting Information) due to the formation of covalent links between the graphene's alkyne groups and the polymer's azide groups that do not impact upon the crystallite size of the graphene nanosheets.

Using different strategies led to entirely different grafting densities and chain lengths of the grafted polymers on the graphene surface, which is directly reflected in the solubility, morphology, and thermal properties of the resulting polymer-FG. Figure 6 shows the grafting density, grafted polymer chain

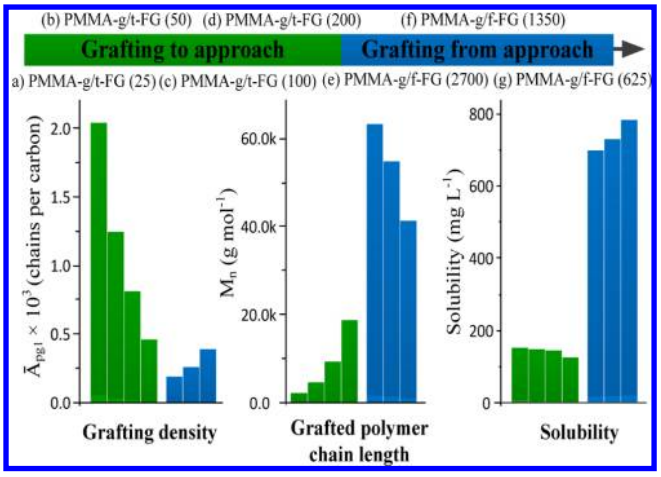

Figure 6. Characterization of PMMA-FG made using two different strategies: (left) 'grafting to' approach and (right) 'grafting from' approach. (See Scheme 1.)

length, and solubility of two functionalized polymers made using different strategies. Whether for 'grafting to' or 'grafting from' approaches, the grafting density is strongly dependent on the grafted polymer's chain length, especially in the 'grafting to' approach. Therefore, we can speculate that steric hindrance from attached polymer chains is the predominant factor influencing the grafting density in both reactions. Although the 'grafting from' approach yields a relatively low grafting density, the chain length of the resulting grafted polymer is still the prime determinant of solubility. Therefore, using the 'grafting from' approach yields longer grafted polymer chains that contribute to polymer solubility in PMMA-g/f-FG.

The X-ray diffraction (XRD) pattern provides evidence of the morphology of the interface layer grafted on the graphene surface, see Figure 7a. As expected, the GO showed a strong peak at 11.8° indicating the presence of functional groups containing oxygen. The GO strong peak is not present in the R-GO pattern, which showed a broad peak at 20.1−30.9,

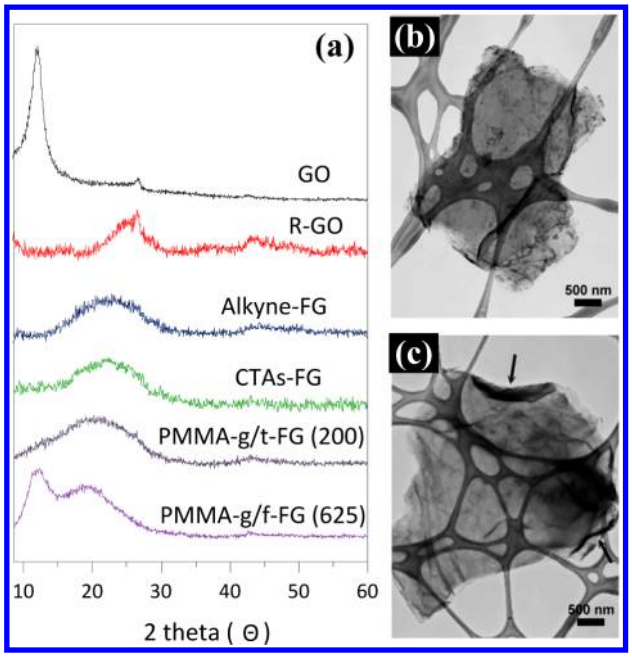

Figure 7. (a) XRD patters of GO, R-GO, alkyne-FG, CTAs-FG, and PMMA-FG powder samples; TEM images of (b) PMMA-g/t-FG (200) and (c) PMMA-g/f-FG (625).

indicating that aggregation occurred during chemical reduction. Covalently grafted APPE, CTAs, and PMMA chains on graphene's surface markedly extended the range of the broad peak to the low-angle position, due to an increase in d-spacing between the graphene sheets. Although the interface space can be markedly increased by grafting polymer on the graphene sheets, contact between neighboring graphene sheets is unavoidable in the absence of sufficient electrostatic repulsion leading to graphene aggregation during the drying process. However, it is worth noting that the strong peak at 12.2° in the PMMA-FG found in the 'grafting from' approach was not present in material made by the 'grafting to' approach. We speculate that longer grafted PMMA chains formed better packed interface layers than shorter grafted PMMA chains giving more uniform interface layers. TEM results (Figure 7b and c) also show the morphological differences between the 'grafting to' and 'grafting from' approaches for PMMA-FG. Dark elliptical spots on the graphene surface are ubiquitous and reveal the morphology of the grafted PMMA chains. This morphology is similar to the case of polymer-FG,[22,23] where polymer aggregates (granular domains) are created on the graphene surface during drying. For the PMMA-g/t-FG (200), the distribution of PMMA, as gray surface granules, appeared uniform. However, the granular contrast observed in PMMA-g/t-FG (200) became barely distinguishable with the long grafted polymer chain of PMMA-g/f-FG (625), where discrete granules were absent. However, the long polymer chains also increased the aggregation tendency at the graphene edges, leading to a folded morphology (marked by the black arrows in Figure 7c).

The effect of the grafted polymer's chain length is also reflected in the difference in the thermal properties of PMMA-FG. Figure S11, Supporting Information, shows TGA curves for PMMA-g/t-FG (200) and PMMA-g/f-FG (625) with corresponding T_{10} values (10 wt % loss temperature). The PMMA-g/f-FG (625) showed a 45.5 °C increase in T_{10} compared to PMMA-g/t-FG (200) with a similar grafting density. This result can explained as longer PMMA grafted polymer chains formed

dx.doi.org/10.1021/cm301345r | Chem. Mater. 2012, 24, 2987−2997

better packed layers and inhibited the decomposition of residual graphene groups more effectively. The glass transition temperature (T_g) also shows the effect of different chain lengths of grafted polymer. The PMMA-g/t-FG (200) and PMMA-g/f-FG (625) showed a 14.9 °C and a 7.8 °C increase in T_g compared to pure PMMA (T_g = 112.2 °C), respectively. This result indicates a substantial confinement effect from the graphene nanosheets on the segmental motion of PMMA chains. Generally, segments in closer proximity to the substrate or the particle surface experience stronger confinement relative to those segments farther away.[65] Hence, shorter PMMA chains on PMMA-g/t-FG showed a higher increase in T_g than the longer grafted polymer chains of PMMA-g/f-FG. Therefore, we believe that the effect of the grafted polymer's chain length on the solubility and thermal properties might predominate in PMMA-FG.

As mentioned, grafting, either by 'grafting to' or 'grafting from', improves the solubility and dispersion of PMMA-FG in several organic solvents such as acetone, THF, DMF, and $CHCl_3$. Therefore, the resulting PMMA-FG can be readily blended with linear PMMA in organic solvents to form polymer-graphene composites. In this study, PMMA-FG was dispersed in $CHCl_3$ and then mixed with PMMA solutions with a 1.5 wt % graphene content, followed by drop-casting to prepare polymer−graphene films. The TEM images (Figure S12, Supporting Information) show that incorporation of PMMA-FG, prepared either by 'grafting to' or 'grafting from', in PMMA generates fully exfoliated graphene nanosheets that can be used directly as a nanofiller to improve the processability and performance of polymer matrices.

Extension of the Grafting Strategy to Various Polymer-Functionalized Graphene. The PMMA-FG cases have shown the differences in grafting characteristics, morphologies, and the resulting solubility of materials made using two grafting strategies, thus paving the way for the production of individually dispersible graphene based materials. To demonstrate the generality of two grafting strategies, we conducted experiments to extend it to other common polymers, including PS, PMAA, P4VP, PDMA, and poly(ethyl glycol) (PEG) (Table S6, Supporting Information). For the 'grafting to' approach, various polymer-N_3 were first prepared by RAFT polymerization, revealing polymer-N_3 formation to be well-controlled as judged by the narrow molecular weight distributions. To understand the effect of different polymer-N_3 and vinyl monomer compositions on the grafting reaction, polymer-N_3 controls, having similar chain lengths (M_n = 8600−11200 g mol^{-1}), but varying molecular weights were used to rule out the possibility that the molecular weight has a significant effect on the grafting reaction. It is noteworthy that all polymer-FG formed by the 'grafting to' approach shows a similar grafting ratio (52.0−54.5 wt %) and grafting density, that is, 6.64−8.21 chains per 10 000 carbons (Table S8, Supporting Information), under the same grafting reaction conditions, indicating that structural differences do not affect the grafting reaction. Additionally, FTIR results provide further information about the corresponding characteristic structures appended to the surface of graphene sheets (shown in Figure S13, Supporting Information).

Various solvents were used to test the solubility of the polymer-FG: the results are shown in Figure 8. The solubility of the original polymer (polymer-N_3) was also tested in a series of solvents, see Table S13, Supporting Information. Clearly, the solubility of the resulting polymer-FG is strongly dependent on

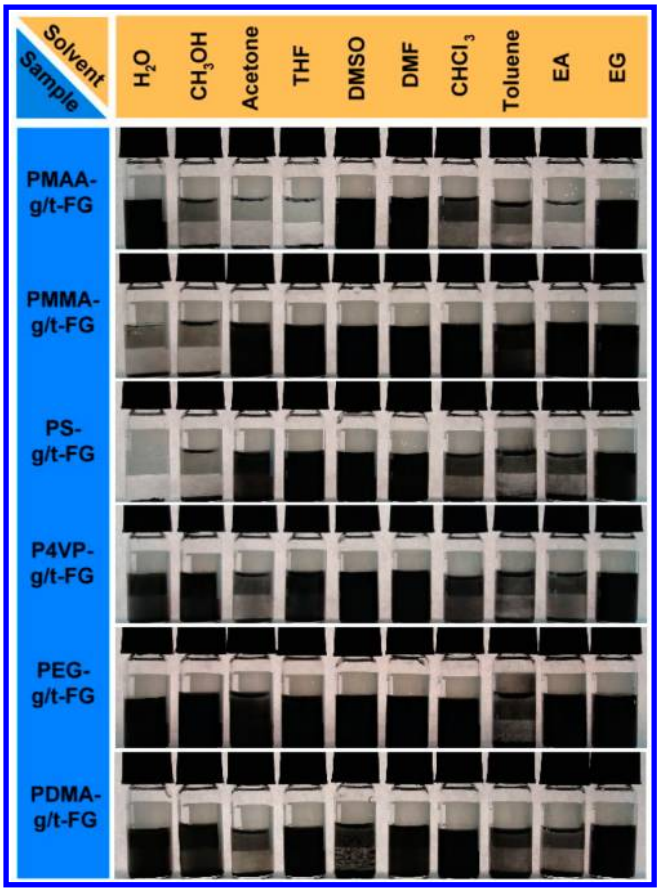

Figure 8. Photographs of polymer-g/t-FG macromolecular brushes in various solvents.

the nature of the grafted polymer; for example, it shows a solubility that is largely consistent with that of the original polymer in its ungrafted state. Therefore, the solubility properties of polymer-FG can be adjusted from water-soluble to oil-soluble, acidic to basic, polar to apolar by selecting a suitable polymer for grafting.

For the 'grafting from' approach, all vinyl monomers can be polymerized by using CTAs-FG with a controlled initiator concentration. GPC results (Table S11, Supporting Information) showed that the M_n of the resulting polymer-graphene ranged from 42100 to 72200 g mol^{-1}, indicating that a high molecular weight was obtained by using this approach. The variation in the molecular weight of these monomers in the presence of CTAs-FG might be explained by steric hindrance originating from the various polymeric propagating radicals on the graphene's surface. Although higher molecular weights can be obtained, the high molecular weight product showed a grafting density (1.33−2.64 chains per 10000 carbons) (Table S11, Supporting Information), that is, approximately one-third that of the polymer-FG formed by the 'grafting to' approach (6.64−8.21 chains per 10000 carbons) (Table S8, Supporting Information). This result is consistent with the observation, namely, that the 'grafting from' approach can achieve a longer grafted polymer chain length for polymer-FG relative to the 'grafting to' approach.

CONCLUSION

This report details powerful and reliable strategies that combines RAFT and click chemistry for the scalable synthesis

of graphene-based molecular brushes. Materials made by different strategies have been evaluated with respect to solubility, morphology and thermal properties. These powerful tools gave control over the grafted polymer's chain length, architecture, grafting ratio and density on the graphene surface in both the 'grafting to' and 'grafting from' approaches. When optimizing the structure and properties of polymer-functionalized graphene for specific applications, graphene dispersion and interface tailoring are crucial and are closely related to the density and chain length of grafted polymer. The use of the 'grafting to' approach offers several advantages compared to the 'grafting from' approach; for example, it gives rise to well-defined and controlled grafted polymer chains, good processability, and high grafting density (note: grafting density decreases with an increase in the chain length of the grafted polymer). However, the 'grafting from' approach allows high molecular weight polymer chains to be appended to surface of graphene, thereby maintaining an adequate grafting density. The polymer-functionalized graphene formed by the 'grafting from' approach yields longer grafted polymer chains, thereby effectively improving the polymer's solubilizing strength. These versatile grafting approaches to graphene-based molecular brushes can be extended to prepare many other distinctive types of polymer-functionalized graphene, opening a new horizon in the field of functional graphene materials.

EXPERIMENTAL SECTION

Chemicals and Materials. Graphite (average particle size 100 μm) was obtained from Fluka. Methyl acrylate (MAA, 99%), methyl methacrylate (MMA ≥98.5%), styrene (St ≥99%), 4-vinylpyridine (4VP 95%), and dimethylamino ethyl methacrylate (DMA 98%), all from Aldrich, were dried and distilled prior to use. 3-azidopropyl 4-cyano-4-((phenylcarbonothioyl)thio) butanoate (azido-CTAs) and *p*-aminophenyl propargyl ether (APPE) were synthesized according to a previously published report.[40] 2,2′-azobis-(2-methylpropionitrile) (AIBN, 98% from Aldrich) was recrystallized twice prior to use. 1,8-diazabicyclo[5.4.0]undec-7-ene (DBU, 98% from Aldrich), copper(I) iodide (Cu (I), 98% from Sigma-Aldrich), and sodium dodecylbenzene sulfonated (SDBS, ≥99.0% from Sigma-Aldrich) were used as received. N, N′-dimethylformamide (DMF, 94%) and chloroform ($CHCl_3$, ≥99%) sullied by Aldrich were dried and distilled prior to use.

General Procedure for the Synthesis of Alkyne-FG. The density of the alkyne groups on the graphene sheets during the diazonium addition was controlled by changing various reaction conditions, for example, (1) the content of *p*-aminophenyl propargyl ether (APPE), (2) the surfactant, and (3) the degree of solvent participation (Scheme S1, Supporting Information). In a typical experiment (without surfactant) (Table S1, Supporting Information, codes 2−4), GO (1 g) was dispersed in 250 mL deionized water. After stirring and sonication for 30 min, hydrazine hydrate (50%, 5 mL) was slowly added to the suspension, which was refluxed at 100 °C for 1 h. Subsequently, APPE (2−4 g) and isoamyl nitrite (2−4 mL) were added, and the mixture was stirred continuously at 80 °C overnight. After cooling to room temperature, the suspension was filtered using DMF until the filtrate was clear. The resulting black solid (alkyne-FG) was dried under vacuum. For comparison 2, alkyne-FG (with surfactant) was synthesized and purified using a similar procedure (Table S1, Supporting Information, code 5), the difference being the addition of 2.5 g surfactant (sodium dodecylbenzene sulfonate, SDBS) with the GO and deionized water. For the bulk state (Table S1, Supporting Information, code 1), the reduced graphene (R-GO) was prepared by using hydrazine hydrate at 100 °C for 1 h and filtering using deionized water to wash. The resulting black solid (R-GO) was dried under vacuum. Subsequently, R-GO was mixed with 20 g of APPE, and the temperature slowly increased 80 °C. After stirring for 30 min at 80 °C, isoamyl nitrite (5 mL) was added, and the mixture was stirred continuously overnight. Alkyne-FG (bulk state) was purified according to the procedure described previously.

Synthesis of CTAs-FG. A 50 mL flask was charged with alkyne functionalized graphene (alkyne-FG) (0.5 g) and DMF (10 mL). Sonication for 30 min at room temperature resulted in the formation of a black suspension, to which 3-azidopropyl 4-cyano-4-((phenylcarbonothioyl) thio) butanoate (azido-CTAs; CTAs-N_3) (0.6 g, 1.66 mmol), Cu (I) (0.16 g, 0.83 mmol) and 1,8-diazabicyclo[5.4.0] undec-7-ene (DBU) (6.31 g, 41.5 mmol) were added. The reaction mixture was evacuated and refilled with nitrogen three times, followed by stirring under argon at 25 °C for 24 h. Then, the mixture was diluted with 200 mL THF, bath-sonicated for 10 min, and filtered through a 200 nm PTFE membrane. The resulting black solid was washed thoroughly with THF (5 × 50 mL), methanol, aqueous ammonium hydroxide solution (28%), water, methanol, and then dried under vacuum overnight (Scheme S1, Supporting Information).

General Procedure for RAFT Polymerization of Vinyl Monomers with Azido-CTAs. Polymerizations were conducted in DMF using AIBN as the primary radical source and azido-CTA as the functional chain transfer agent. In typical polymerization (run 2 of Table S2, Supporting Information), MMA (3 g, 30.0 mmol, 50 equiv), azido-CTAs (0.217 g, 0.6 mmol, 1.0 equiv), and AIBN (2.09 g, 0.12 mmol, 0.2 equiv) were added to a glass tube with a magnetic stirring bar, and then, DMF was added until the total concentration was 4 M. The tubes were subjected to three cycles of freeze−pump−thaw to remove oxygen. The tube was subsequently immersed into an oil bath preheated to 70 °C. After 24 h, the polymerization was quenched by placing the tube into an ice−water bath. The polymerization solution was drawn and dissolved into $CDCl_3$ for ^1H NMR, which revealed the monomer conversion to be 95.6%, by comparing the integrated areas of the characteristic signals of the monomer and polymer. After precipitating into a large amount of methanol, azido-terminated PMMA was isolated, and its molecular weight and polydispersity (PDI) were obtained by gel permeation chromatography (GPC) in Table S2, Supporting Information. Other polymers were synthesized according to a similar approach and summarize the experimental results in Table S3, Supporting Information.

General Procedure for Click Reaction of Polymer-N_3 to Alkyne-FG Using the 'Grafting to' Approach. The PMMA grafting ratio on the graphene sheets, during the click reaction, was controlled by changing (1) the concentration and molecular weight of polymer-N_3, (2) DBU participation, and (3) the reaction time (Scheme S3, Supporting Information). In a typical experiment, a 50 mL flask was charged with alkyne-FG (50 mg) and DMF (10 mL). Sonicating for 30 min at room temperature, led to the formation of a black suspension, to which azide-functionalized PMMA [PMMA-N_3 (100); M_n (GPC) = 9600 g mol^{-1}] (0.2 g, 0.019 mmol) was added. The reaction mixture was evacuated and refilled with nitrogen three times, followed by stirring under argon at 60 °C for 24 h. Following which PMMA-functionalized graphene (PMMA-FG) was purified in a similar way to CTAs-FG, as described. The PMMA-FG preparation conditions examined are given in Tables S4 and S5, Supporting Information. Other polymer-functionalized graphene composites (PS-g/t-FG, PMAA-g/t-FG, P4VP-g/t-FG, PDMA-g/t-FG, and PEG-g/t-FG) were synthesized with the same conditions (Table S5, Supporting Information, code 3) and purified using the same procedure, while Table S6, Supporting Information, tabulates grafting ratios when PMMA-N_3 was replaced by the corresponding azido-terminated polymer (polymer-N_3).

General Procedure for the RAFT Polymerization of Vinyl Monomers with CTAs-FG Using the 'Grafting from' Approach. All polymerizations were conducted in DMF using AIBN as the primary radical source and CTAs-FG as the functional chain transfer agent. The ratios of the monomer and initiator (AIBN), together with the reaction times, are listed in Table S9, Supporting Information. In a typical polymerization (code 1−4), a glass tube with a magnetic stirring bar, was charged with CTAs-FG (10 mg) and DMF (5 mL). After sonicating for 30 min at room temperature, a black suspension formed, and MMA (5 g) and AIBN (3.04 mg) ([M]/[AIBN] = 2700) were added. The tubes were subjected to three cycles of freeze−

pump−thaw to remove oxygen. The tubes were subsequently immersed into an oil bath preheated to 70 °C. After 8 h, the polymerization was quenched by placing the tubes into an ice−water bath. Then, the mixture was diluted with 200 mL THF, bath-sonicated for 10 min, and filtered through a 200 nm PTFE membrane. The black solid was washed thoroughly with THF (5 × 50 mL), methanol, and chloroform (5 × 10 mL) and then dried under vacuum overnight (Scheme S4, Supporting Information). PMMA-g/f-RGO was synthesized using a similar approach [Table S10, Supporting Information, code 1]. Other polymer-functionalized graphenes (PS-g/f-FG, PMAA-g/f-FG, P4VP-g/f-FG, and PDMA-g/f-FG) were synthesized using a similar procedure, with alterations in the washing solvent as appropriate (Table S11, Supporting Information).

Characterization. FTIR spectra were obtained with a Nicolet Avatar 320 FTIR spectrometer; 32 scans were collected at a spectral resolution of 1 cm^{-1}. The sample for FTIR measurement was prepared by deposition of solutions on salt plates. Solid state ^{13}C NMR spectra were recorded on a Buuker-400 MHz instrument using tetramethylsilane as an internal reference. The XPS measurements were performed with ESCA 2000 (VG Microtech) using a monochromatized Al Kα anode. The internal solvent peak was used to calibrate the chemical shift in the NMR data. A HITACHI L-7100 pump, a RI 2000 refractive index detector (Schambeck SFD GmbH) with an elution rate of 1.0 mL min^{-1} at a temperature of 80 °C with a Polymer Laboratories PLgel guard column (5 μm particles; 50 × 7.5 mm) and a PLgel 5 μm mixed-D column (300 × 7.5 mm; particle size, 5 μm,) were connected in series. The molecular weight calibration curve was obtained using poly(ethylene oxide) standards of defined molecular weight (1010−163 000 g mol^{-1}) (Polymer Laboratories Inc., MA). For GPC characterization of the hydrolysis sample, the polymer-FG was dispersed in DMF prior to hydrolysis. After hydrolysis, the products in DMF were filtered and used directly for GPC measurements. Raman spectra were measured on a Renishaw RM1000 multichannel confocal microspectrometer with 633 nm laser excitation. The UV−vis spectra were obtained using a Mecasys Optizen 2120 UV spectrometer at room temperature. The morphology of the graphene in the composites was observed using a JEOL JEM-1200CX-II transmission electron microscope operated at 120 kV. X-ray diffraction (WAXD) spectra were recorded on powdered samples using a Rigaku D/max-2500 type X-ray diffraction instrument. The thermal degradation behavior of the membranes was measured using a Q50 thermogravimetric analyzer (TGA) operated from room temperature to 850 °C at a heating rate of 20 °C min^{-1} under a nitrogen atmosphere. The glass transition temperature (T_g) was measured using differential scanning calorimetry (DSC) with a DuPont TA Instrument Q20 controller.

■ ASSOCIATED CONTENT

Ⓢ Supporting Information

XPS and ^{13}C NMR of GO and R-GO; FTIR, XPS, ^{13}C NMR, TGA, and TEM of polymer-FG. This material is available free of charge via the Internet at http://pubs.acs.org.

■ AUTHOR INFORMATION

Corresponding Author

*E-mail: bjh@mail.ntust.edu.tw.

Notes

The authors declare no competing financial interest.

■ REFERENCES

(1) Kim, H.; Abdala, A. A.; Macosko, C. W. *Macromolecules* **2010**, *43*, 6515.
(2) Verdejo, R.; Bernal, M. M.; Romasanta, L. J.; Lopez-Manchado, M. A. *J. Mater. Chem.* **2011**, *21*, 3301−3310.
(3) Cao, Y.; Liu, S.; Shen, Q.; Yan, K.; Li, P.; Xu, J.; Yu, D.; Steigerwald, M. L.; Nuckolls, C.; Liu, Z.; Guo, X. *Adv. Funct. Mater.* **2009**, *19*, 2743.
(4) Yamaguchi, H.; Murakami, K.; Eda, G.; Fujita, T.; Guan, P.; Wang, W.; Gong, C.; Boisse, J.; Miller, S.; Acik, M.; Cho, K.; Chabal, Y. J.; Chen, M.; Wakaya, F.; Takai, M.; Chhowalla, M. *ACS Nano* **2011**, *5*, 4945.
(5) Dua, V.; Surwade, S. P.; Ammu, S.; Agnihotra, S. R.; Jain, S.; Roberts, K. E.; Park, S.; Ruoff, R. S.; Manohar, S. K. *Angew. Chem., Int. Ed.* **2010**, *49*, 2154.
(6) Kwon, S.-Y.; Ciobanu, C. V.; Petrova, V.; Shenoy, V. B.; Bareño, J.; Gambin, V.; Petrov, I.; Kodambaka, S. *Nano Lett.* **2009**, *9*, 3985.
(7) Park, S.; Mohanty, N.; Suk, J. W.; Nagaraja, A.; An, J.; Piner, R. D.; Cai, W.; Dreyer, D. R.; Berry, V.; Ruoff, R. S. *Adv. Mater.* **2010**, *22*, 1736.
(8) Wang, Y.; Li, Z.; Hu, D.; Lin, C.-T.; Li, J.; Lin, Y. *J. Am. Chem. Soc.* **2010**, *132*, 9274.
(9) Lahiri, J.; Miller, T.; Adamska, L.; Oleynik, I. I.; Batzill, M. *Nano Lett.* **2010**, *11*, 518.
(10) Mattevi, C.; Kim, H.; Chhowalla, M. *J. Mater. Chem.* **2011**, *21*, 3324.
(11) Green, A. A.; Hersam, M. C. *Nano Lett.* **2009**, *9*, 4031.
(12) Yu, G.; Hu, L.; Vosgueritchian, M.; Wang, H.; Xie, X.; McDonough, J. R.; Cui, X.; Cui, Y.; Bao, Z. *Nano Lett* **2011**, *11*, 2905.
(13) Stankovich, S.; Dikin, D. A.; Dommett, G. H. B.; Kohlhaas, K. M.; Zimney, E. J.; Stach, E. A.; Piner, R. D.; Nguyen, S. T.; Ruoff, R. S. *Nature* **2006**, *442*, 282.
(14) Xu, L. Q.; Yang, W. J.; Neoh, K.-G.; Kang, E.-T.; Fu, G. D. *Macromolecules* **2010**, *43*, 8336.
(15) Zhu, Y.; Higginbotham, A. L.; Tour, J. M. *Chem. Mater.* **2009**, *21*, 5284.
(16) Jang, J.-H.; Rangappa, D.; Kwon, Y.-U.; Honma, I. *J. Mater. Chem.* **2011**, *21*, 3462−3466.
(17) Potts, J. R.; Lee, S. H.; Alam, T. M.; An, J.; Stoller, M. D.; Piner, R. D.; Ruoff, R. S. *Carbon* **2011**, *49*, 2615.
(18) Yang, X.; Ma, L.; Wang, S.; Li, Y.; Tu, Y.; Zhu, X. *Polymer* **2011**, *52*, 3046.
(19) He, H.; Gao, C. *Chem. Mater.* **2010**, *22*, 5054.
(20) Fang, M.; Wang, K.; Lu, H.; Yang, Y.; Nutt, S. *J. Mater. Chem.* **2009**, *19*, 7098.
(21) Pan, Y.; Bao, H.; Sahoo, N. G.; Wu, T.; Li, L. *Adv Funct Mater* **2011**, *21*, 2754.
(22) Fang, M.; Wang, K.; Lu, H.; Yang, Y.; Nutt, S. *J. Mater. Chem.* **2010**, *20*, 1982.
(23) Kan, L.; Xu, Z.; Gao, C. *Macromolecules* **2010**, null.
(24) Shan, C.; Yang, H.; Han, D.; Zhang, Q.; Ivaska, A.; Niu, L. *Langmuir* **2009**, *25*, 12030.
(25) Zhang, B.; Chen, Y.; Zhuang, X.; Liu, G.; Yu, B.; Kang, E.-T.; Zhu, J.; Li, Y. *J. Polym. Sci. Part A: Polym. Chem.* **2010**, *48*, 2642.
(26) Chandra, V.; Yu, S. U.; Kim, S. H.; Yoon, Y. S.; Kim, D. Y.; Kwon, A. H.; Meyyappan, M.; Kim, K. S. *Chem. Commun.* **2012**, *48*, 735.
(27) Salavagione, H. J.; Martínez, G. *Macromolecules* **2011**, *44*, 2685.
(28) Yang, Y.; Wang, J.; Zhang, J.; Liu, J.; Yang, X.; Zhao, H. *Langmuir* **2009**, *25*, 11808.
(29) Liu, Y.; Yao, Z.; Adronov, A. *Macromolecules* **2005**, *38*, 1172.
(30) Xu, Z.; Gao, C. *Nat. Commun.* **2011**, *2*, 571.
(31) Xu, Z.; Gao, C. *ACS Nano* **2011**, *5*, 2908.
(32) Paredes, J. I.; Villar-Rodil, S.; Martínez-Alonso, A.; Tascón, J. M. D. *Langmuir* **2008**, *24*, 10560.
(33) Dyke, C. A.; Tour, J. M. *J. Am. Chem. Soc.* **2003**, *125*, 1156.
(34) Jin, Z.; McNicholas, T. P.; Shih, C.-J.; Wang, Q. H.; Paulus, G. L. C.; Hilmer, A. J.; Shimizu, S.; Strano, M. S. *Chem. Mater.* **2011**, *23*, 3362−370.
(35) Sinitskii, A.; Dimiev, A.; Corley, D. A.; Fursina, A. A.; Kosynkin, D. V.; Tour, J. M. *ACS Nano* **2010**, *4*, 1949.
(36) Zhu, Y.; Tour, J. M. *Nano Lett.* **2010**, *10*, 4356.
(37) Kolb, H. C.; Finn, M. G.; Sharpless, K. B. *Angew. Chem., Int. Ed.* **2001**, *40*, 2004.
(38) Mansfeld, U.; Pietsch, C.; Hoogenboom, R.; Becer, C. R.; Schubert, U. S. *Polym. Chem.—U.K.* **2010**, *1*, 1560.
(39) Sumerlin, B. S.; Vogt, A. P. *Macromolecules* **2009**, *43*, 1.
(40) Ye, Y.-S.; Shen, W.-C.; Tseng, C.-Y.; Rick, J.; Huang, Y.-J.; Chang, F.-C.; Hwang, B.-J. *Chem. Commun.* **2011**, *47*, 10656−10658.

(41) Ye, Y.-S.; Yen, Y.-C.; Cheng, C.-C.; Syu, Y.-J.; Huang, Y.-J.; Chang, F.-C. *Polymer* **2010**, *51*, 430.
(42) Tasdelen, M. A.; Van Camp, W.; Goethals, E.; Dubois, P.; Du Prez, F.; Yagci, Y. *Macromolecules* **2008**, *41*, 6035.
(43) Xu, Z.; Gao, C. *Macromolecules* **2010**, *43*, 6716.
(44) Kou, L.; He, H.; Gao, C. *NanoMicro Lett.* **2010**, *2*, 177−183.
(45) Xu, F. J.; Yang, W. T. *Prog. Polym. Sci.* **2011**, *36*, 1099.
(46) Lowe, A. B.; McCormick, C. L. *Prog. Polym. Sci.* **2007**, *32*, 283.
(47) Tseng, C.-Y.; Ye, Y.-S.; Cheng, M.-Y.; Kao, K.-Y.; Shen, W.-C.; Rick, J.; Chen, J.-C.; Hwang, B.-J. *Adv. Energy Mater.* **2011**, *1*, 1220−1224.
(48) Ye, Y.-S.; Tseng, C.-Y.; Shen, W.-C.; Wang, J.-S.; Chen, K.-J.; Cheng, M.-Y.; Rick, J.; Huang, Y.-J.; Chang, F.-C.; Hwang, B.-J. *J. Mater. Chem.* **2011**, *21*, 10448.
(49) Xie, L.; Xu, F.; Qiu, F.; Lu, H.; Yang, Y. *Macromolecules* **2007**, *40*, 3296.
(50) Jung, I.; Dikin, D.; Park, S.; Cai, W.; Mielke, S. L.; Ruoff, R. S. *J. Phys. Chem. C* **2008**, *112*, 20264.
(51) Stankovich, S.; Dikin, D. A.; Piner, R. D.; Kohlhaas, K. A.; Kleinhammes, A.; Jia, Y.; Wu, Y.; Nguyen, S. T.; Ruoff, R. S. *Carbon* **2007**, *45*, 1558.
(52) Gao, C.; Vo, C. D.; Jin, Y. Z.; Li, W.; Armes, S. P. *Macromolecules* **2005**, *38*, 8634.
(53) Sinani, V. A.; Gheith, M. K.; Yaroslavov, A. A.; Rakhnyanskaya, A. A.; Sun, K.; Mamedov, A. A.; Wicksted, J. P.; Kotov, N. A. *J. Am. Chem. Soc.* **2005**, *127*, 3463.
(54) Fan, X.; Peng, W.; Li, Y.; Li, X.; Wang, S.; Zhang, G.; Zhang, F. *Adv. Mater.* **2008**, *20*, 4490.
(55) Kudin, K. N.; Ozbas, B.; Schniepp, H. C.; Prud'homme, R. K.; Aksay, I. A.; Car, R. *Nano Lett.* **2007**, *8*, 36.
(56) Calizo, I.; Balandin, A. A.; Bao, W.; Miao, F.; Lau, C. N. *Nano Lett* **2007**, *7*, 2645.
(57) Pimenta, M. A.; Dresselhaus, G.; Dresselhaus, M. S.; Cancado, L. G.; Jorio, A.; Saito, R. *Phys. Chem. Chem. Phys.* **2007**, *9*, 1276.
(58) Bodine, K. D.; Gin, D. Y.; Gin, M. S. *J. Am. Chem. Soc.* **2004**, *126*, 1638.
(59) Qin, S.; Qin, D.; Ford, W. T.; Resasco, D. E.; Herrera, J. E. *Macromolecules* **2004**, *37*, 752.
(60) Bahr, J. L.; Mickelson, E. T.; Bronikowski, M. J.; Smalley, R. E.; Tour, J. M. *Chem. Commun.* **2001**, 193.
(61) Kan, L.; Xu, Z.; Gao, C. *Macromolecules* **2010**, *44*, 444.
(62) Long, J.; Fang, M.; Chen, G. *J. Mater. Chem.* **2011**, *21*, 10421.
(63) Lee, S. H.; Dreyer, D. R.; An, J.; Velamakanni, A.; Piner, R. D.; Park, S.; Zhu, Y.; Kim, S. O.; Bielawski, C. W.; Ruoff, R. S. *Macromol. Rapid Commun.* **2010**, *31*, 281.
(64) Cao, Y.; Lai, Z.; Feng, J.; Wu, P. *J. Mater. Chem.* **2011**, *21*, 9271.
(65) Oh, H.; Green, P. F. *Nat. Mater.* **2009**, *8*, 139.